Supporting Information

Design of Refolding DNA Aptamer on Single-Walled Carbon Nanotubes for Enhanced Optical Detection of Target Proteins

Kwan Lee[‡]*, Jeeyeon Lee[§], and Byungmin Ahn[‡†]*

[‡] Department of Energy Systems Research and [†] Department of Materials Science and Engineering, Ajou University, Suwon 16499, Republic of Korea

[§] Institute for Health Innovation & Technology (iHealthtech), National University of Singapore, Singapore 117599, Singapore

Table of Contents

Materials and Methods

Figure S1. Schematic comparison of wrapping methods for the periodically sequenced ssDNA-SWNT hybrids.

Figure S2. 3D fluorescence response mapping of SC-SWNT hybrids.

Figure S3. Solvatochromic shift of SC-SWNT hybrids and surface coverage calculation methods

Figure S4. Reversibility of PBA-SWNT hybrids in an alginate hydrogel

Figure S5. UV-Vis-NIR absorption spectra of IBA-SWNT, $(TAT)_6$-SWNT, IBA-$(TAT)_6$-SWNT hybrids

Figure S6. Solvatochromic shift of $(TAT)_6$-SWNT hybrids

Figure S7. Relative fluorescence response of the $(TAT)_6$-SWNT hybrids with BSA

Figure S8. Relative fluorescence response of the IBA-$(TAT)_6$-SWNT hybrids with BSA

Figure S9. Fitting using Stern-Vomer model formulation.

Figure S10. UV-Vis-NIR absorption spectra change of the IBA-$(TAT)_6$-SWNT hybrids by insulin

Figure S11. Circular dichroism (CD) spectra of IBA-$(TAT)_6$-SWNT hybrids

Figure S12. Relatively normalized intensities from (9,5) nanotubes of PBA-SWNT, $(AT)_9$-SWNT and PBA-$(AT)_9$-SWNT hybrids

Figure S13. Circular dichroism (CD) spectra of PBA-$(AT)_9$-SWNT hybrids

Figure S14. Relative fluorescence response of $(GT)_n$-SWNT hybrids with BSA

Figure S15. Fluorescence response of PBA-$(GT)_n$-SWNT hybrids (n = 1 and 12) by PDGF-BB

Figure S16. Fluorescence response of IBA-SWNT hybrids without consecutive centrifuging processes

Figure S17. Fluorescence response of IBA-SWNT hybrids with consecutive centrifuging processes by buffer solution and BSA

Figure S18. Relative surface coverage modulation of IBA-SWNT hybrids by insulin

Materials and Methods

Preparation of SC-SWNT hybrids samples. Single-walled carbon nanotubes using CoMoCAT and HiPCO were suspended with 2 wt% sodium cholate (SC) in 10 mL of deionized water by tip ultra-sonicating (3 W for 90 min) in an ice bath. The resultant aqueous suspension of SC-SWNT hybrids was centrifuged to remove undispersed powders at 30,000 g for 1 h. After carefully gathering the 80% supernatant of SC-SWNT hybrids suspension, the centrifugation under the identical condition was repeated to remove precipitants, which was typically performed by 3 or 4 times.

Tip sonication for DNA-SWNT hybrids. For 1μg/μL solution of DNA-SWNT hybrids suspension, as-produced SWNTs was mixed with aqueous DNA solution with molar ratio (DNA/SWNT =2). The identical procedure for SC-SWNT hybrids was performed.

Ligand exchange of SC-SWNT to *Aptamer-SWNT* and *Aptamer-Anchor-SWNT* hybrids. DNA aptamer was suspended in 100 mM NaCl solution. The SC-SWNT hybrids suspension was mixed with DNA aptamer suspension with a molar ratio (e.g. DNA/SC-SWNT = 5). The mixture was dialyzed using a 5 kDa molecular weight cutoff dialysis tube (Spectrum Laboratories, Inc.) against 100 mM NaCl solution (4 L) for at least 24 h while severally exchanging the solution. To remove free DNA from the solution, the second dialysis was performed using a 100 kDa molecular weight cutoff dialysis tube (Spectrum Laboratories, Inc.) against 100 mM NaCl solution (4 L) for at least 24 h while exchanging the solution.

Ligand exchange of SC-SWNT to *Aptamer-SWNTs* hybrids with the consecutive centrifuges. DNA aptamer was suspended in 100 mM NaCl solution. The SC-SWNT hybrid suspension was mixed with DNA aptamers suspension with a molar ratio (e.g. Aptamer/SWNT = 5). The mixture was dialyzed using a 5 kDa molecular weight cutoff dialysis tube (Spectrum Laboratories, Inc.) against 100 mM NaCl solution (4 L) for at least 24 h while severally exchanging the solution. After *Dialysis-I*, the centrifuge was applied for 60 min under 10,000 rpm and the 80% supernatant was transferred to a dialysis tube. To remove free DNA from the suspension, the second dialysis was performed using a 100 kDa molecular weight cutoff dialysis tube (Spectrum Laboratories, Inc.) against 100 mM NaCl solution (4 L) for at least 24 h while exchanging the solution. After *Dialysis-II*, the second centrifuge was performed for 1 h under 10,000 rpm. The supernatant of the 80% volume was taken and transferred for heating and aging for 24 h. The centrifuge for 1 h under 10,000 rpm was performed and the supernatant of 80% volume was taken for optical characterization and the optical sensing modulation.

Concentration calculation: (1) SC-SWNT hybrids: UV-Vis-NIR absorption spectra characterized the concentration of SC-SWNT hybrids with a weight extinction coefficient of 0.0465 L mg^{-1} cm^{-1} at 808 nm, which enable to adjust to 20 mg/L of SC-SWNT hybrids

concentration in 2 wt% SC solution as a stock suspension, which was kept at room temperature. (2) Ligand exchange of SC-SWNT to Aptamer-SWNT hybrids: The resulting suspensions of DNA aptamer-SWNT hybrids were analyzed by UV-Vis-NIR spectroscopy. The UV-Vis-NIR absorption spectra determined the concentration of DNA aptamer-SWNT hybrids, which used to adjust to 20 mg/L as a stock suspension using 100 mM NaCl solution and it was kept at refrigerator (4 ℃).

Preparation of *Aptamer-SWNT* hybrids in alginate hydrogels: The mixture of 10 wt% sodium alginate solution and 5 mg/L of Aptamer-SWNT hybrids suspension was cross-linked by addition of a solution containing calcium ions for 2 h.

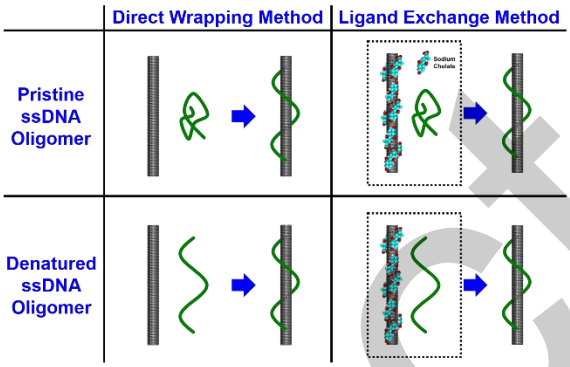

Figure S1. Schematic comparison of wrapping methods for the periodically sequenced ssDNA-SWNT hybrids using pristine and denatured ssDNA. The description shows the direct wrapping using tip-sonication and the indirect wrapping procedure through two-steps dialysis for ligand exchange between sodium cholate and ssDNA, in which "Pristine ssDNA Oligomer" represents the untreated pristine ssDNA (e.g. $(TAT)_n$, $(AT)_n$, and $(GT)_n$) and the pretreatment of the pristine ssDNA oligomers for denaturation by heating and cooling down expressed as "Denatured ssDNA Oligomer".

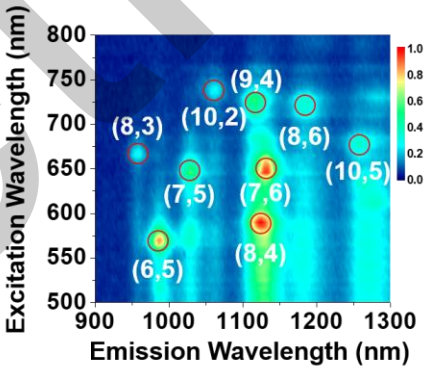

Figure S2. 3D mapping of fluorescence emission of nanotube species with (n,m) nanotubes of the SC-SWNT hybrids.

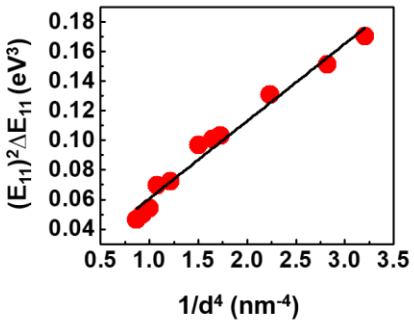

Figure S3. Solvatochromic shift $(E_{11})^2\Delta E_{11}$ of SC-SWNT hybrids against the nanotube diameter to the power of negative 4 (~$1/d^4$) for the various chiralities. The local dielectric environment of the single-walled carbon nanotube surface influences the radiative decay of excitons, which correspond to the solvent Stark effect of the fluorescent emission peaks. The environmentally induced dipole moment of SWNTs by a dipolar solvent causes electric field polarizability between the excited and ground state, which generate the solvatochromic shift ($E_{ii}^2\Delta E_{ii}$) of the optical transition energies (E_{ii}) and the difference of the optical transition energy (ΔE_{ii}) between the dielectric environmental DNA-SWNT hybrids and pristine SWNTs in air as solvent Stark effect.[1,2] The solvatochromic shift is proportional to the Onsager polarity function (f(x) = 2(x-1)/(2x-1)) using the solvent dielectric constant (ε) and refractive index (η), a fluctuation constant (L), scaling constant (k) of the SWNTs polarizability, and the carbon nanotube radius (R) by

$$E_{ii}^2\Delta E_{ii} = \left(E_{ii}^{Air}\right)^2\left(E_{ii}^{Air} - E_{ii}^{DNA\ aptamer}\right) = -Lk\left[\frac{2(\varepsilon-1)}{2\varepsilon+1} - \frac{2(\eta^2-1)}{2\eta^2+1}\right]\left(\frac{1}{R^4}\right) = \frac{C}{R^4} \qquad (1)$$

All other parameters except diameter can be represented by C because of the constant feature for a specific chirality. The optical transition energy in air (E_{ii}^{Air}) was estimated using Planck's constant (h), the speed of light (c), the diameter of SWNTs (d), the chiral angle (θ) regarding (n,m) chiralities by

$$E_{11}^{air}[eV] = \frac{hc}{A_1+A_2 d} + A_3\frac{cos3\theta}{d^2} = \frac{1242}{61.1+1113.6d} + A_3\frac{cos3\theta}{d^2} \qquad (2)$$

Here, the mod((n-m),3) of a chiral index determine $A_3 = -0.077$ eV/nm^2 (mod3 = 1) and $A_3 = 0.032$ eV/nm^2 (mod3 = 2). The solvatochromic shift is plotted against the SWNT diameter to the power of negative 4 as ($1/d^4$) for the various chiralities in each wrapping condition within an identical solvent (e.g. PBS buffer solution with 1 mM $MgCl_2$). The linear fitting for the data provides the slope of the fit curves and the corresponding R-square parameters, in which The effective dielectric constant (ε_{eff}) near the SWNTs can be estimated by comparing a reference system.

$$\left(E_{11}^{Air}\right)^2\left(E_{11}^{Air} - E_{11}^{DNA\ aptamer}\right) = \frac{C}{R^4} = \frac{C'}{d^4} \qquad (3)$$

Regarding surface coverage of DNA on SWNTs, it is reported that the solvatochromic shift from an individual SWNTs diameter enables the calculation of the average surface coverage using the effective dielectric constant by assuming a linear combination of the surrounding water and the DNA wrapping contribution ($\varepsilon_{effective} = \alpha\varepsilon_{DNA} + (1-\alpha)\varepsilon_{water}$, where α is the relative surface coverage

of SWNT by DNA, $\varepsilon_{DNA} = 4$, and $\varepsilon_{water} = 88.1$).[1–3] In addition, the energy difference of fluorescence spectra from the DNA-SWNT hybrid is correlating to the DNA surface coverage difference on (n,m) nanotube, in which the red-shift fluorescence of DNA-SWNT hybrids represents the sparser DNA coverage and the blue-shifting indicates the denser coverage.[4,5]

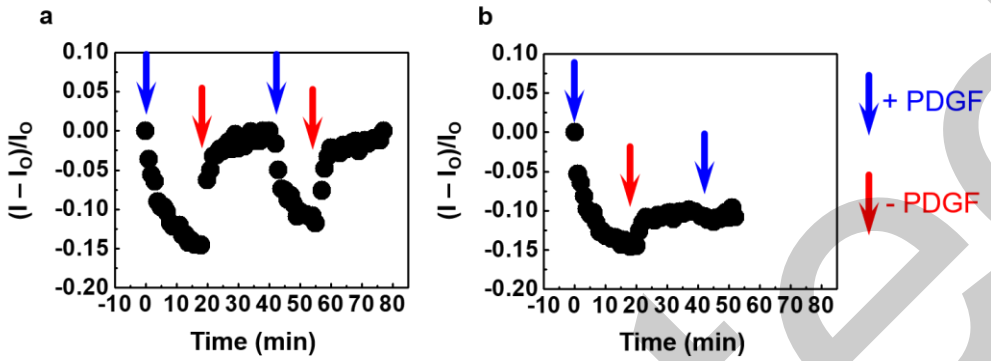

Figure S4. Reversibility of PBA-SWNT hybrids in an alginate hydrogel. (a) Reversible fluorescence response of (9,4) nanotubes at 1124 nm from the indirectly wrapped PBA-SWNT hybrids when the alternative exchange of buffer containing 0.08 nM (blue) and 0 nM (red) of PDGF-BB. (b) No reversible fluorescence response from directly wrapped PBA-SWNT hybrids because of PBA detachment from the SWNTs.

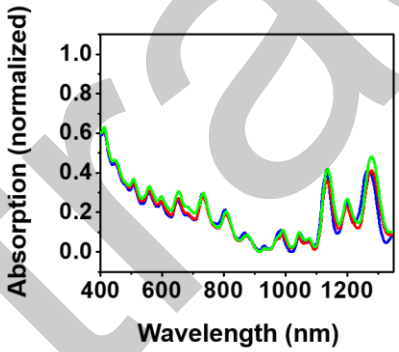

Figure S5. UV-Vis-NIR absorption spectra of IBA-SWNT (blue), IBA-$(TAT)_6$-SWNT (red) and $(TAT)_6$-SWNT (green) hybrids suspension.

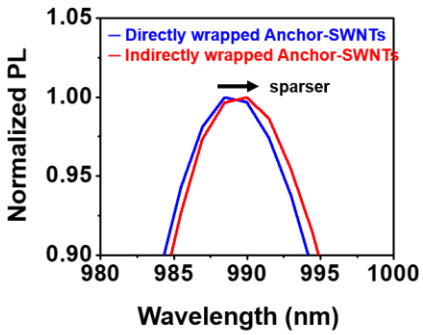

Figure S6. Solvatochromic shift of (6,5) nanotube for $(TAT)_6$-SWNT hybrids by the direct wrapping method (blue) and the ligand exchange approach as the indirect wrapping method (red).

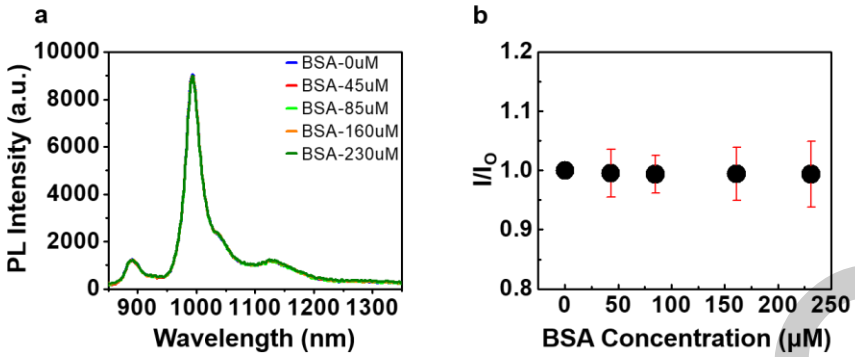

Figure S7. (a) Fluorescence spectra and (b) relative fluorescence response of $(TAT)_6$-SWNT hybrids with the increasing concentration of bovine serum albumin (BSA). The relative response is analyzed with the maximum PL peak intensities from (6,5) nanotube of $(TAT)_6$-SWNT hybrids.

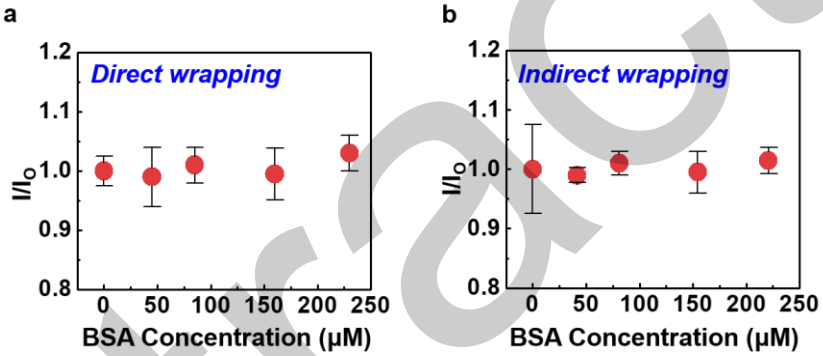

Figure S8. Relative fluorescence response of (a) the directly wrapping and (b) the indirectly wrapping for the IBA-$(TAT)_6$-SWNT hybrids with the increasing concentration of bovine serum albumin (BSA). The relative response is analyzed with the maximum PL peak intensities from (6,5) nanotube of the IBA-$(TAT)_6$-SWNT hybrids.

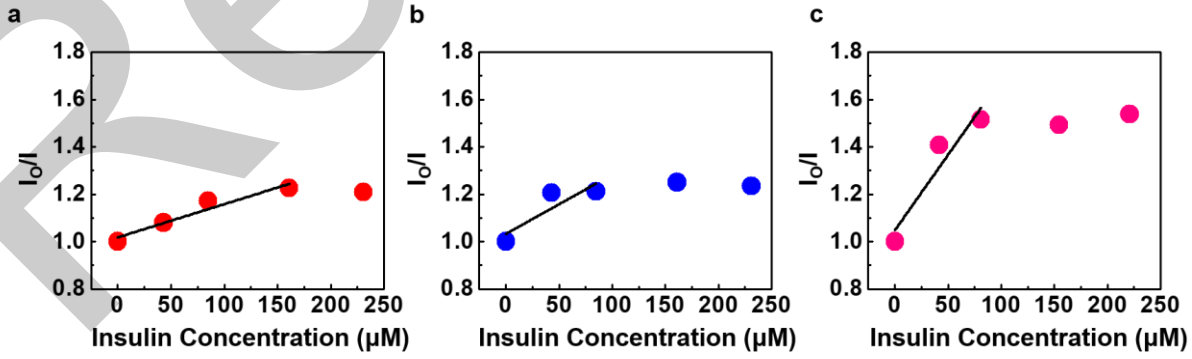

Figure S9. Fitting using Stern-Vomer model formulation for (a) directly wrapped IBA-SWNT, (b) indirectly wrapped IBA-SWNT, and (c) directly wrapped IBA-$(TAT)_6$-SWNT hybrids with the increase of insulin concentration except when the I_O/I value is saturated. It was reported that the predominant PL quenching kinetics can be understood with constant PL quenching rate (k_q) resulting from photoinduced charge transfer as the predominant quenching mechanism. ($I_O/I = 1 + k_q\tau_0$, assuming PL lifetime of 20 ps without a quencher (τ_0)).[6]

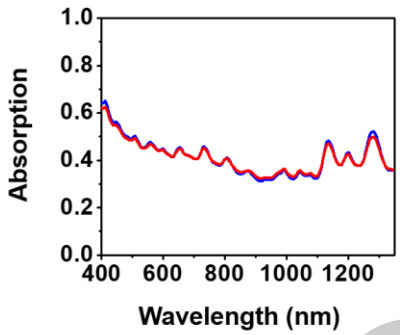

Figure S10. UV-Vis-NIR absorption spectra of IBA-$(TAT)_6$-SWNTs hybrids before (blue) and after (red) the addition of 200 μM insulin.

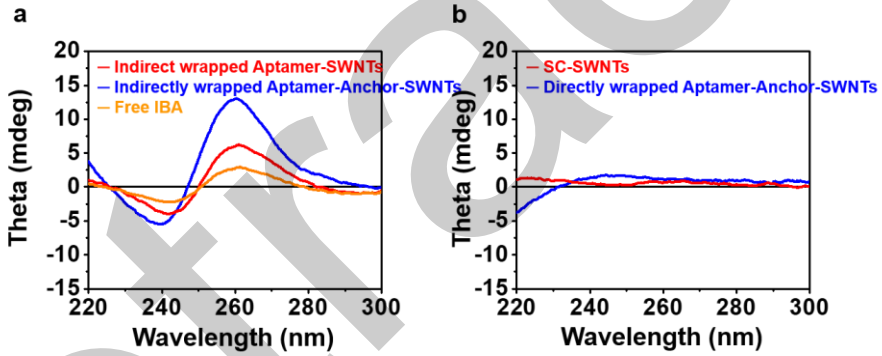

Figure S11. Circular dichroism (CD) spectra of (a) the indirectly wrapped IBA-SWNTs (red) and IBA-$(TAT)_6$-SWNTs hybrids (blue) showing a parallelly four-stranded G-quadruplex structure of free IBA (orange) in buffer solution which is consistent to previous report,[6] and (b) SC-SWNTs (red) and directly wrapped IBA-$(TAT)_6$-SWNT hybrids (blue) without a specific structures.

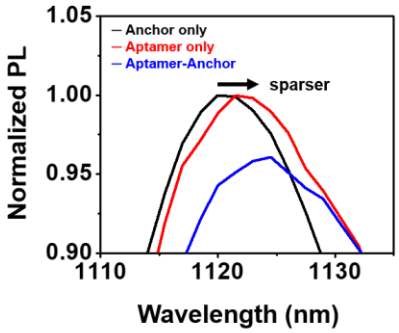

Figure S12. Relatively normalized intensities at maximum peak of PBA-SWNT, $(AT)_9$-SWNT and PBA-$(AT)_9$-SWNT hybrids. Regarding solvatochromic shift from (9,5) nanotubes, the higher surface coverage of $(AT)_9$-SWNT hybrids are observed and the PBA-$(AT)_9$-SWNT hybrids shows sparser relative surface coverage than other two hybrids.

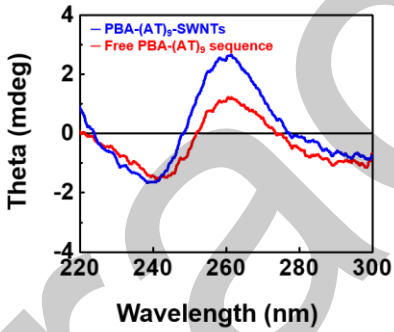

Figure S13. Circular dichroism (CD) spectra of the indirectly wrapped PBA-$(AT)_9$-SWNTs (blue) and free DNA of PBA-$(AT)_9$ (red) in buffer solution show a parallelly four-stranded G-quadruplex structures.

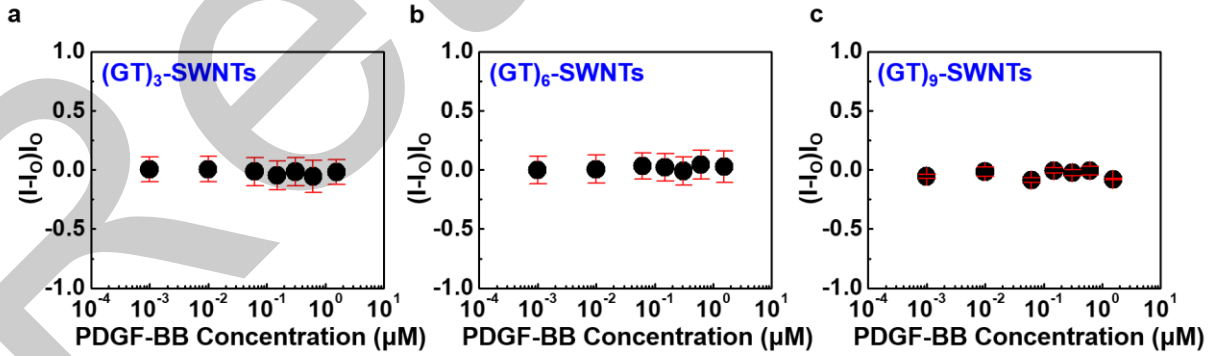

Figure S14. Relative fluorescence response of $(GT)_n$-SWNT hybrids to PDGF-BB with (a) n =3, (b) n = 6, and (c) n = 9.

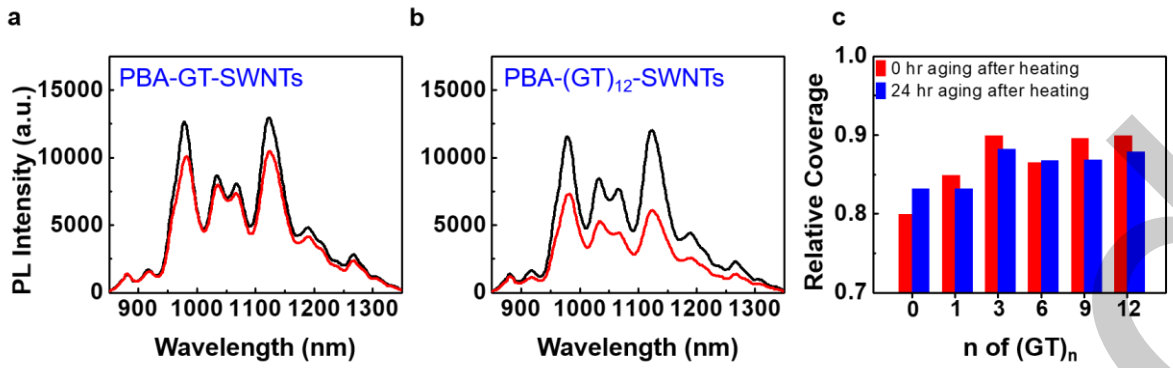

Figure S15. Fluorescence spectra modulation of (a) PBA-GT-SWNT and (b) PBA-$(GT)_{12}$-SWNT hybrids by the addition of PDGF-BB (0.08 nM) to compare anchor lengths with $(GT)_n$ (n = 3, 6, and 9). (c) Relative surface coverage with different length of anchoring phase $(GT)_n$ (where, n = 0, 1, 3, 6, 9, and 12)

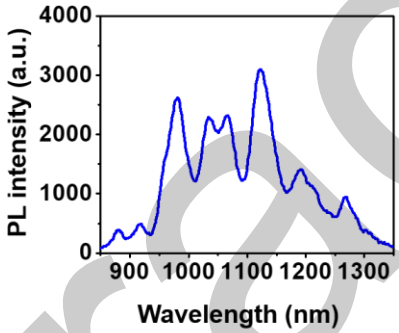

Figure S16. Fluorescence emission from the indirectly wrapped IBA-SWNT hybrids (using HiPco) under the excitation of 785 nm wavelength. Without the centrifuging process, the fluorescence emission from higher chiralities of SWNTs (e.g. (10,5) and (12,2) nanotubes) are probed.

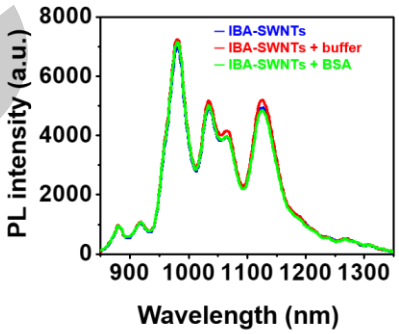

Figure S17. Fluorescence spectra of IBA-SWNT hybrids (blue) with the consecutive centrifuging process. No fluorescence modulation by the addition of buffer solution (red) and 85 μM BSA (green).

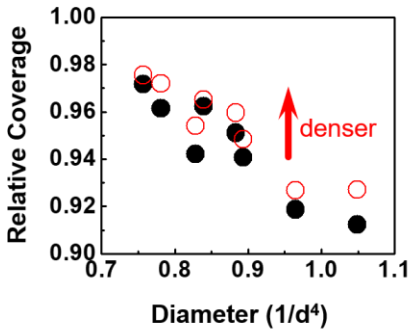

Figure S18. Relative surface coverage modulation when insulin binds to the IBA-SWNT hybrids prepared with indirect wrapping followed by the consecutive centrifuging. The various chiralities show the denser surface coverage after the insulin addition (red open dot) comparing the pristine IBA-SWNT hybrids (black close dot).

References

(1) Choi, J. H.; Strano, M. S. Solvatochromism in Single-Walled Carbon Nanotubes. *Appl. Phys. Lett.* **2007**, *90* (22), 223114. https://doi.org/10.1063/1.2745228.

(2) Bisker, G.; Dong, J.; Park, H. D.; Iverson, N. M.; Ahn, J.; Nelson, J. T.; Landry, M. P.; Kruss, S.; Strano, M. S. Protein-Targeted Corona Phase Molecular Recognition. *Nat. Commun.* **2016**, *7*, 10241. https://doi.org/10.1038/ncomms10241.

(3) Heller, D. A.; Jeng, E. S.; Yeung, T.-K.; Martinez, B. M.; Moll, A. E.; Gastala, J. B.; Strano, M. S. Optical Detection of DNA Conformational Polymorphism on Single-Walled Carbon Nanotubes. *Science* **2006**, *311* (5760), 508–511. https://doi.org/10.1126/science.1120792.

(4) Lee, K.; Nojoomi, A.; Jeon, J.; Lee, C. Y.; Yum, K. Near-Infrared Fluorescence Modulation of Refolded DNA Aptamer-Functionalized Single-Walled Carbon Nanotubes for Optical Sensing. *ACS Appl. Nano Mater.* **2018**, *1* (9), 5327–5336. https://doi.org/10.1021/acsanm.8b01377.

(5) Jeng, E. S.; Moll, A. E.; Roy, A. C.; Gastala, J. B.; Strano, M. S. Detection of DNA Hybridization Using the Near-Infrared Band-Gap Fluorescence of Single-Walled Carbon Nanotubes. *Nano Lett.* **2006**, *6* (3), 371–375. https://doi.org/10.1021/nl051829k.

(6) Cha, T.-G.; Baker, B. A.; Sauffer, M. D.; Salgado, J.; Jaroch, D.; Rickus, J. L.; Porterfield, D. M.; Choi, J. H. Optical Nanosensor Architecture for Cell-Signaling Molecules Using DNA Aptamer-Coated Carbon Nanotubes. *ACS Nano* **2011**, *5* (5), 4236–4244. https://doi.org/10.1021/nn201323h.